



# Inertial Navigation – Importance of Initial Heading: A Constrained Dual GNSS Receiver Approach

Lukas Blocher, Tobias Hiller, Wolfram Mayer, Joachim Gerlach, Oliver Bringmann

**Abstract**—This paper describes scenarios for automated driving which are highly relevant on accurate initial heading estimation. We show thoughtfully designed experiments which are closely aligned with real world demands to explain the relevance and influence of initial heading estimation. We conclude that purely inertial navigation is highly dependent on accurate initial heading. On the basis of these experiments we show a constrained dual GNSS receiver approach which takes advantage of short baselines and known receiver baseline length to estimate initial heading without relying on the Earth’s magnetic field.

**Index Terms**—IMU, inertial navigation, GNSS, GPS, initial heading, compass, dual receiver, constrained

## I. INTRODUCTION

Current developments in automated driving show a continuous extension of the operation design domain to lower and higher speeds as well as more challenging environments. Since an automated vehicle is basically a mobile robot, both applications share the common fundamental task of navigation. *Navigation* is the job of making a plan from a start to a destination and therefore requires determining the current position, a process called *localization* [7, p.241]. This work deals with the importance of one special component of localization: *Initial heading*. Localization is the basic building block of every mobile robot [8, p.385], therefore the heading component deserves special attention to provide a sophisticated foundation for further enhancements in automated driving and high level decision making.

### A. Initial Heading

Heading is part of an attitude solution determining the rotation with respect to a given coordinate frame. Attitude includes three rotation angles: yaw/heading, pitch and roll [6, p.32]. While pitch and roll can be estimated by using the gravity vector, heading  $\psi$  requires special treatment since external reference and separate sensors are required to determine heading relative to north. Such references may be a compass or a GNSS

Lukas Blocher, Tobias Hiller, Wolfram Mayer, Robert Bosch GmbH. Joachim Gerlach, gerlach@hs-albsig.de, Albstadt-Sigmaringen University. Oliver Bringmann, oliver.bringmann@uni-tuebingen.de, University of Tuebingen.

receiver. A compass may be challenged by magnetic field fluctuations caused by electric drives whereas a single GNSS receiver may only deliver heading when using a trajectory at least two consecutive, sufficiently spaced, samples. To address these challenges this work relies on a dual GNSS receiver approach to be able to determine heading without any magnetic reference in low speed and standstill situations. In this context the term *initial* denotes two special scenarios which are highly relevant when *real* autonomy of robots is desired:

1) *System Cold Start*: Start of a mobile robot without any prior knowledge of heading while being at standstill.

2) *Purely Inertial Navigation Start*: The robot is moving along a trajectory with known heading. At the described point in time continuous heading determination is becoming impossible due to the GNSS reference system being unavailable. The last known heading needs to be extrapolated by using inertial sensors.

### B. Inertial Navigation

Inertial sensors are self-contained and therefore not dependant on any external source. Consequently this type of sensor does require an exact knowledge of initial position and attitude at start when used for a navigation task. Without having a global reference the knowledge of position relative to a starting point is a challenging task [7, p.242]. An extrapolation of position is done by integrating angular rate from three gyroscopes and acceleration from three accelerometers relative to a starting point. Special attention is brought to inertial navigation when a robot enters a GNSS denied environment or faces system degradation and therefore loses its absolute positioning reference. The challenge is to initialize an inertial navigation system properly, especially in the initial heading scenarios listed above.

### C. Approach

The following sections explains the relevance of initial heading and the defined scenarios by first focusing on purely inertial navigation. The experiments clearly show the influence and importance of a reliable and

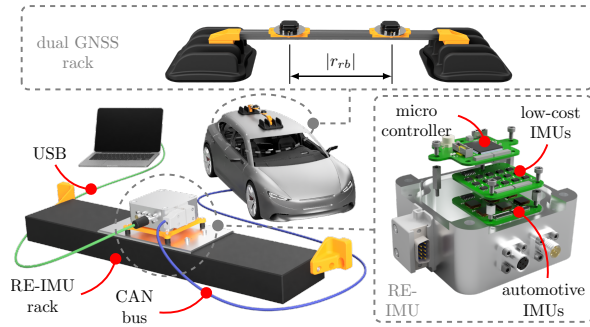


Figure 1. [3] ©IEEE 2022. Rendering of the setup for our experiments built around the redundant IMU (RE-IMU), which is mounted on a rack in the trunk of a vehicle. The RE-IMU is connected to vehicle CAN bus to acquire wheel speed information. *Detail, right*: exploded view of the RE-IMU showing its sub-components. *Detail, top*: Dual GNSS antenna rack for ground truth and heading acquisition.

Table I  
TOTAL MEAN OF MEASURED GYROSCOPE ANGLE RANDOM WALK (ARW) AND BIAS INSTABILITY (BIS) FOR ALL SENSORS COMBINED IN THE RE-IMU AS EXPLAINED IN [3][4].

Parameter	$x$ -axis	$y$ -axis	$z$ -axis	Unit
ARW	2.06	2.36	1.54	[mdps/rtHz]
BIS	0.40	0.68	0.46	[dph]

accurate heading information for the previously defined scenarios. On the basis of the conclusion in II, the concept of the dual GNSS receiver approach is explained to address the previously discovered challenges for initial heading estimation.

## II. IMPORTANCE OF INITIAL HEADING

This first section focuses on inertial navigation and explains the relevance of heading in this context. As concluded in our previous work purely inertial navigation with low-cost MEMS IMUs is only relevant for real-world applications for short periods of time. Therefore we introduced augmentation with vehicle odometry from wheel speed sensors. In our previous work purely inertial navigation and addressing stochastic and deterministic errors with different sensor array configurations is explained more detailed in [2] [3]. This work summarizes the previous conclusions and reconsiders them within the use-case of automated driving. The approach of this section is called gyroscope-assisted odometry (GAO) which receives velocity information from wheel-speed sensors while calculating relative heading from angular rates. In this case one integration step can be removed compared to purely inertial navigation and the duration of usable navigation can be extended.

### A. Setup

The experiment setup is built around the redundant IMU (RE-IMU). It has to be stated that for this work

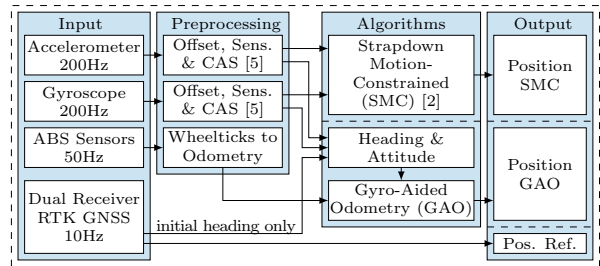


Figure 2. [3] ©IEEE 2022. Block diagram of data-processing. Pre-measurement calibration is executed to reset gyroscope offset, normalize accelerometer data and to calculate attitude. Vehicle wheel ticks are converted to distance and velocity. GNSS is used for reference trajectory and initial heading initialisation during calibration.

the exact sensor configuration within the IMU is of minor importance, more information may be obtained from [3]. The RE-IMU is also responsible for CAN data acquisition and data streaming to a laptop. The IMU is rigidly mounted to the trunk of the vehicle while sitting on vibration dampers, as shown in Fig. 1. The micro controller within the RE-IMU handles sensor SPI data communication, data streaming via USB and also collecting wheel tick information from the ESP system. We took care to allow high speed and precisely synchronized 50Hz wheel tick data acquisition. Additionally two multi-band GNSS antennae with a baseline length of 32 cm are mounted to the roof of the vehicle. Two uBlox F9P GNSS receivers are linked in moving baseline configurations and therefore are able to provide heading information. Additionally the receiver positions are corrected by SAPOS HEPS real time kinematic service. The usage of RTK improves absolute positioning for allowing precise ground truth acquisition. While RTK improves absolute positioning, heading is not very sensitive to errors in position [9]. The GNSS setup allows sub-10 cm absolute positioning and sub- $0.5^\circ$  heading acquisition at high rate.

### B. Theory

1) *Inertial Sensors*: The output of the RE-IMU can be treated as one high performance MEMS IMU due to taking the mean of all 14 sensor samples resulting in enhanced noise performance. The detailed architecture and IMU data fusion is described in [2]. Additional sensor array architectures were analysed in [11]. The sensor fusion of the individual IMUs result in angle random walk (ARW) and bias instability (BIS) parameters for RE-IMU total output as shown in Tab. I.

2) *Virtual Wheel Model*: The setup uses the rear axle as centre of reference for odometry calculation as discussed by [3] and [10]. The risk of introducing additional wheel slip is reduced by extracting odometry data from the rear axle while using a front wheel drive vehicle. Both rear wheels are considered as one virtual middle wheel in the reference point, while assuming constant velocity between samples. Relative motion

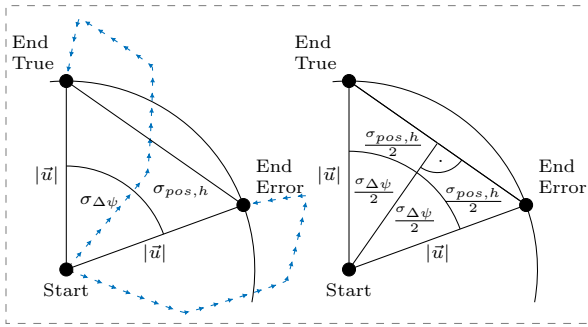


Figure 3. Illustration of the influence of initial heading on the scenario as shown in Figure 4. The initial heading error  $\Delta\psi$  and the distance between start and endpoint  $|\vec{u}|$  directly influence position error on the endpoint.

heading is provided integrating gyroscope angular rate output.

3) *Initial heading and Attitude*: Initial heading and attitude are fundamental components to be able to make use of the odometry data. A coordinate transformation is required to transform odometry data from the body frame to the navigation frame based on current attitude. The discussed signal flow is shown in Fig. 2. To determine the initial attitude, the gravity vector is derived from accelerometer data. Using the initial attitude as a starting point continuous attitude is maintained by integrating angular rates. As illustrated in Fig. 3 the initial heading error  $\Delta\psi$  together with the distance between start and endpoint  $|\vec{u}|$  directly influence position error on the end point. The initial heading position error component  $\sigma_{pos,h}$  is time invariant and given by

$$\sigma_{pos,h}(|\vec{u}|) = 2|\vec{u}| \sin\left(\frac{\sigma_{\Delta\psi}}{2}\right). \quad (1)$$

The error contribution of z-axis gyroscope  $\sigma_{pos,g}$  resulting from ARW  $N_z$  and BIS  $B_z$  is dependent on both time  $t$  and average vehicle velocity  $\bar{v}$

$$\sigma_{pos,g}(t, \bar{v}) = \bar{v} \sqrt{(2N_z \sqrt{t^3}/3)^2 + (B_z t^2/2)^2}. \quad (2)$$

Since both components  $\sigma_{pos,h}$  and  $\sigma_{pos,g}$  are stochastically independent the resulting total position error is defined as

$$\sigma_{pos}(t, \bar{v}, |\vec{u}|) = \sqrt{\sigma_{pos,g}(\bar{v}, t)^2 + \sigma_{pos,h}(|\vec{u}|)^2}. \quad (3)$$

4) *Navigation Algorithms*: The data processing in MATLAB is designed as shown in Fig. 2. After sensor data preprocessing and scaling, calibration data and alignment procedures are applied. The mean initial heading from the dual GNSS setup is used for absolute heading alignment during calibration. Applying the initial heading as offset to integrated angular rates results in converting the otherwise relative information to absolute north heading. During vehicle movement the GNSS heading is solely used for generating a reference trajectory for performance evaluation. Additionally the

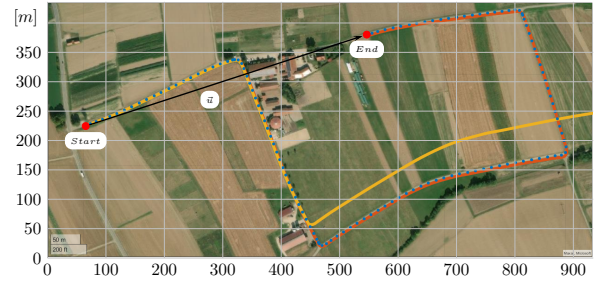


Figure 4. [3] ©IEEE 2022. Comparison of output trajectory of experiment D, shown in Figure 5. *Blue dots*: RTK-corrected GNSS ground truth, *yellow*: motion constrained strap-down, *red*: gyro-aided odometry. The scenario involved a distance travelled of 1600 m between start and end point (*red*) in 275 s.

GNSS samples on the starting point are used to align the relative navigation information to a global map for visualisation.

### C. Experiments

1) *Calibration*: In advance of the experiments the individual IMUs are calibrated using a highly accurate rate table. The first step of data processing applies calibration results to trim scale-factor, offset and cross-axis sensitivity. To achieve high positioning accuracy calibration is inevitable. Additionally the wheel circumference was calibrated using the RTK corrected GNSS setup to determine the distance per wheel tick. Preparatory to each experiment the vehicle standstill is used to determine gyroscope offsets, to calculate pitch/roll angles, to normalize the gravity vector and also to extract initial heading via the dual-antenna GNSS system.

2) *Measurements*: The measurements A to E, shown in Fig. 5 were recorded with the trajectory depicted in Fig. 4. The driven path is 1600 m long at an average speed of  $5.8 \text{ m s}^{-1}$  within 275 s. To generate the reference trajectory one F9P GNSS chipset was configured in dual band and multi-constellation mode as well as fed with network RTK data. An open sky scenario, free from buildings and obstructions was chosen to ensure optimal GNSS signalling conditions and low risk of multipath.

3) *Discussion*: The values of z-axis in Tab. I being  $N_z = 1.54 \text{ mdps/rtHz}$  and  $B_z = 0.46/\sqrt{2 \cdot \ln(2)/\pi} \text{ dph} = 0.69 \text{ dph}$  are used for further predictions. With  $t = 275 \text{ s}$  and  $d = 1600 \text{ m}$  the corresponding mean velocity is  $\bar{v} = 5.8 \text{ m/s}$ . Using Eq. (2) the predicted gyroscope position error is  $\sigma_{pos,g} = 0.88 \text{ m}$ . Since we did not include any reference for initial heading, we assume an error  $\sigma_{\Delta\psi} = 0.4^\circ$  due to observations during our experiments. With  $|\vec{u}| = 505.41 \text{ m}$  the calculated heading error is  $\sigma_{pos,h} = 3.53 \text{ m}$ . The total position error is  $\sigma_{pos} = 3.64 \text{ m}$ , when using Eq. (3). The 2D position error  $|\Delta\vec{d}| = |[x_n \ y_n]|$  between SMC, GAO

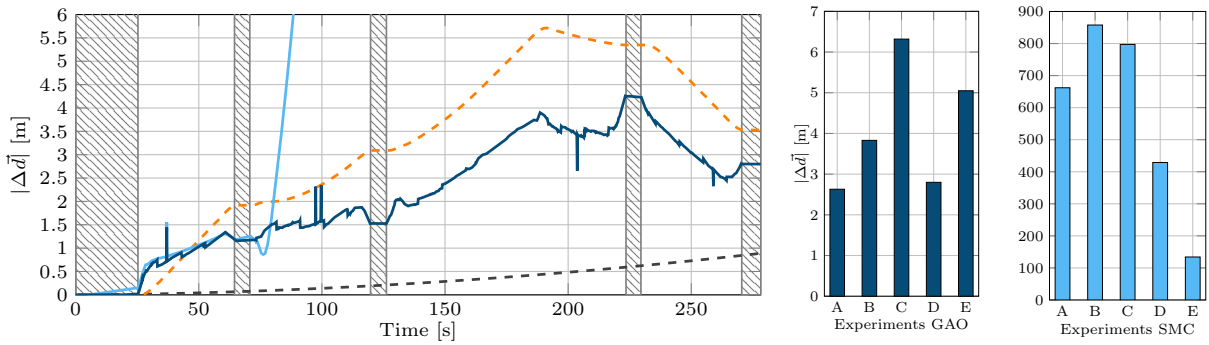


Figure 5. [3] ©IEEE 2022, *Left*: 2D position error plot of SMC (solid, light blue) and GAO (solid, dark blue) compared to the RTK GNSS reference corresponding to experiment D. The plot results from the trajectory shown in Figure 4. Stops at intersections are represented by the hatched grey areas. The predicted position error  $\sigma_{\text{pos},h}$  (dashed, orange) based on the initial heading error decreases when returning closer to the start point. Predicted position error due to gyroscope noise  $\sigma_{\text{pos},g}$  (dashed, grey) grows over time. *Right*: Total error of 5 independent measurements. All trajectories were as shown in Figure 4.

and GNSS reference is shown in Fig. 5. The SMC approach reflects the trajectory pretty well but shows significant error growth after a short period of time. The GAO approach does not suffer from cubic error growth due to the initial heading error being directly dependent of distance between start and end point  $|\vec{u}|$ . For  $t > 230$  s the error decreases since  $|\vec{u}|$  shrinks when closing in on the starting point.

#### D. Conclusion

Compared to a purely inertial approach, the odometry based variant shows greatly improved performance by being independent of accelerometer based velocity. High data rate and precisely synchronized data processing combined with dual-antenna GNSS baseline estimation provide an essential foundation for better navigation results. The measurements try to simulate the scenario “System Cold Start“, defined in Sec. I. By predicting the individual error components we are able to highlight the relevance of initial heading estimation for such a scenario. For our experiment durations initial heading error is dominant over gyroscope error. Additionally we conclude that when not relying on the Earth’s magnetic field, a state of the art dual-antenna GNSS system is suitable to solve for initial heading at standstill. Our observations fully match previous works like [7, P. 244] stating “Especially bad are errors in orientation, because they have the largest effect on position accuracy“.

### III. CONSTRAINED DUAL GNSS RECEIVER APPROACH

Based on the resulting conclusions, the next step is to implement a solution for determining initial heading. Additionally such an approach can be merged with purely inertial navigation to allow continuous heading estimation. To be able to determine heading when at standstill for the scenarios described in the introduction we chose to implement a dual GPS approach with focus on the following criteria: I) short baseline  $< 1$  m,

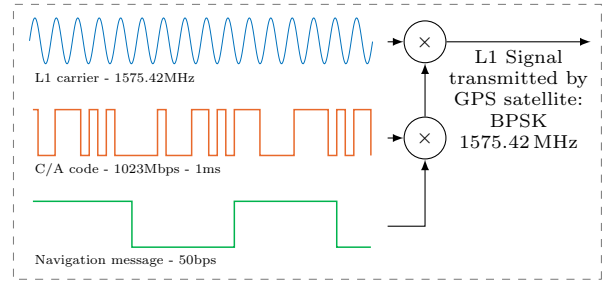


Figure 6. Data is applied to the carrier using BPSK (biphase shift key modulation). Carrier, C/A code and navigation message are combined to generate DSSS (direct spread spectrum) signals within the satellite (not drawn to scale) [13, 9].

II) double differencing for robust relative positioning and III) using the known antenna baseline length as a constraint. The setup consists of two independent GNSS receivers, receiving GPS L1 signals, while being clocked from an individual clock. The corresponding antennae are mounted on a antenna rack fixed to each other, as shown in Fig. 1. This work uses GPS to verify the developed approach which may be extended to other satellite constellations.

#### A. Fundamentals

GPS offers several information sources which are relevant for positioning. The basic one is the carrier wave. Measuring the carrier phase introduces most ambiguity but offers the most precise measurements. Since we are targeting for small baseline the approach shown makes use of the carrier wave, instead of the C/A code, due to the receiver noise being approximately 1 % of the wavelength [14, P. 53]. On top of the carrier wave the C/A code is applied to distinguish the satellites in the constellation. Therefore each satellite broadcasts its individual PRN (pseudo random noise) code. The satellites also provide navigation messages which contain ephemeris data for localizing the satellites in orbit. For this work the ephemeris data are required to determine the satellite line of sight vectors

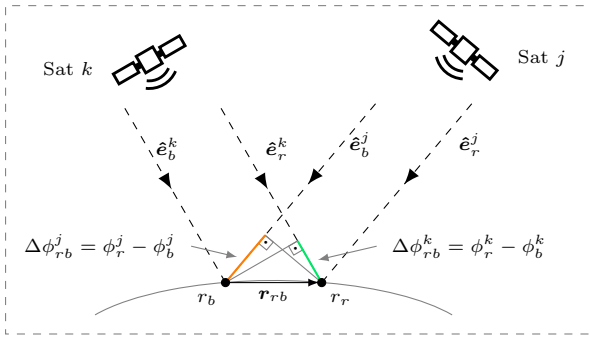


Figure 7. Two single carrier phase differences, as described by [12],[14, p.56]. Double differencing results from subtracting two single differences.

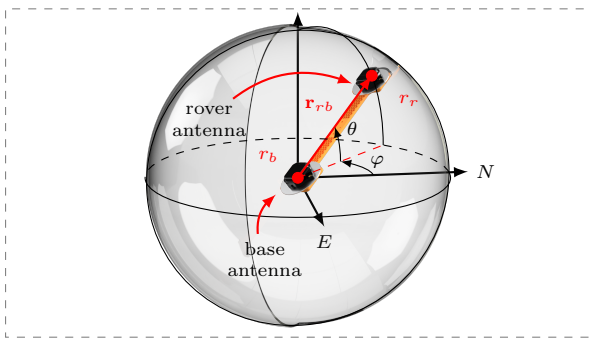


Figure 8. Spherical solution space with rover antenna in the centre of the sphere and radius being the antenna distance or baseline length  $r_{rb}$ . The variables  $\varphi$  and  $\theta$  are estimated, all possible solution candidates are located on the surface of the sphere.

$\hat{e}_b^k$ . Instead of relying on absolute positioning we rely on using the advantage of having two receivers. Therefore relative positioning is possible using a technique called “double differencing“, an explanation in [14, p.58]. The single difference involves observing a satellite from both receivers which eliminates satellite clock errors and signal propagation delays due to atmospheric disturbances. Single differencing is executed by taking the carrier phase measurements of each receiver concerning the same satellite at the same point in time and subtracting them, as shown in Fig. 7. The step to double differencing is done by subtracting two single differences from two satellites  $k$  and  $j$ , consequently removing receiver clock errors if the receivers are synchronized. Double differencing removes hard to determine error sources leading to a very robust but relative output.

### B. Solution Space

Most of the previous approaches try to estimate the baseline vector  $r_{rb}$  with three degrees of freedom  $X$ ,  $Y$  and  $Z$  in a Cartesian coordinate system. This approach uses the known baseline length  $|r_{rb}|$  as a constraint, since it is a-priori knowledge and decreases the size of the solution space. The resulting solution space is a sphere with radius  $|r_{rb}|$ . The base antenna is fixed

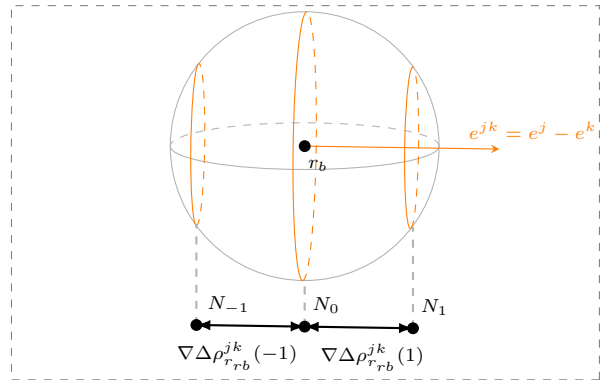


Figure 9. Positioning of the solution candidate circles for the double differenced LOS vector  $e^{jk}$ , when iterating  $N$  to solve for the unknown wavelength ambiguity.

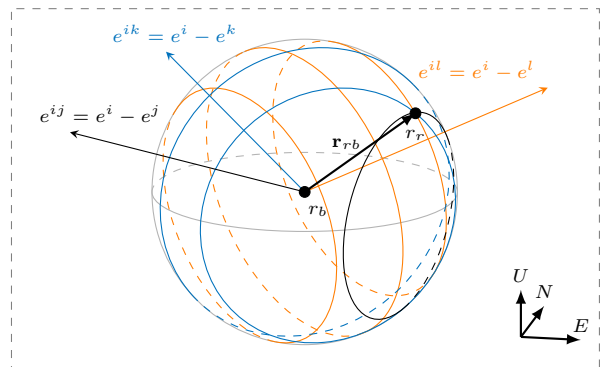


Figure 10. Solution space for 3 pairs of satellites, as shown in Fig. 9. The colors visualize all candidates for one pair of satellites when iterating  $N$ .  $r_r$  marks the point on the sphere surface where one circle of each satellite pair intersects and therefore the desired solution candidate.

in the centre of the sphere while the rover antenna can move on the surface of the sphere. Consequently we are searching for possible solutions in a spherical coordinate system with the two degrees of freedom  $\varphi$  and  $\theta$ , as shown in Fig. 8.

The carrier phase measurements  $\phi$  are geometrically aligned along the direction of the satellite signal represented by the line of sight (LOS) unit vectors  $\hat{e}$ . So double differencing can be considered creating a “virtual“ satellite with the LOS vector  $\hat{e}^j - \hat{e}^k$  and the geometric double difference  $\nabla\Delta\rho_{r_{rb}}^{jk}$  being aligned along it. Due to an ambiguous carrier phase considering multiples  $N$  of the wavelength  $\lambda$  is required. As shown in Fig. 9 this results in multiple circles for each  $N$  with the circles being spaced by  $\lambda$ , scaled with  $\hat{e}^j - \hat{e}^k$ :

$$\nabla\Delta\rho_{r_{rb}}^{jk}(N) = \lambda \frac{(\nabla\Delta\phi_{r_{rb}}^{jk} + \nabla\Delta N_{r_{rb}}^{jk})}{|\hat{e}^j - \hat{e}^k|}. \quad (4)$$

Each virtual satellite generates a group of circles for varying  $N$ , represented by colors in Fig. 9. The solution candidate we are looking for is a point on the sphere surface where one circle of each virtual satellite

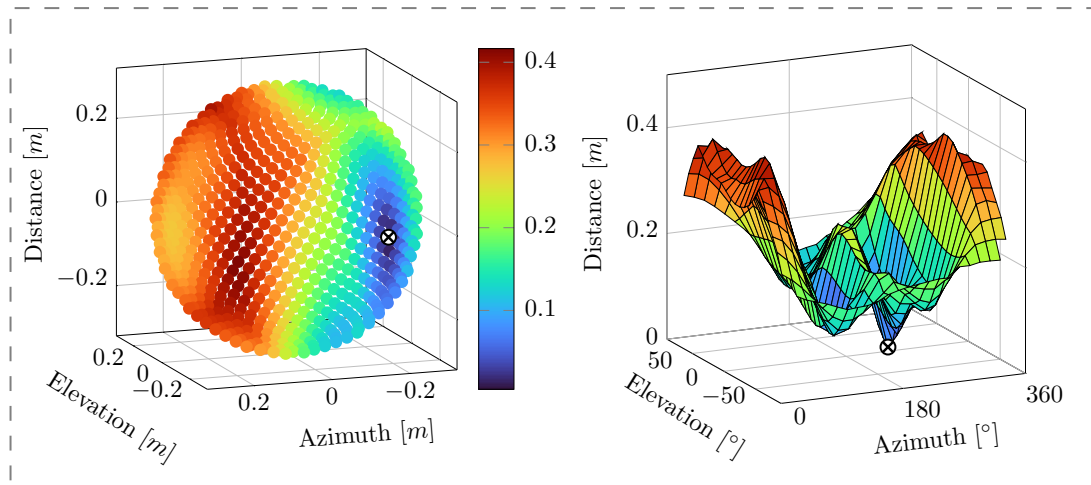


Figure 11. Discretised solution space with points projected onto the sphere surface. For each point the distance to the closest candidate circle, as shown in Fig. 10, is calculated. The resulting metric is the norm distance to each of the circles accumulated. *Left*: Spherical solution space, distance metric visualized by color. *Right*: Equivalent solution space as *left*, but azimuth and elevation angles rolled out in a plane and distance metric visualized on the z-Axis to visualize the distribution of minima.

intersects. The intersection point is the position of the rover antenna  $r_r$  relative to the base.

### C. Simulation

For verifying the described approach, we developed a simulation environment to be able to freeze the highly dynamic satellite constellation and to isolate error sources. For finding a solution for a given scenario and satellite placement we set the baseline length to  $|r_{rb}| = 32\text{ cm}$  and projected a grid of points onto the sphere surface. For each point on the surface we calculated the distance to the closest solution circle to find possible intersection. The point being on or close to a circle of each group is the desired solution. The described approach is visualized in Fig. 9. The colors represent the norm distance to the closest circle of each group. Consequently the lower the metric, the better the potential solution. The dark blue points represent the desired solutions with a low distance metric. Fig. 11 *right* is just another representation of the solution space with azimuth and elevation angles  $\varphi$ ,  $\theta$  being rolled out in a plane. The Z-Axis represents the distance metric and therefore the distribution of minima is more obvious.

### D. Conclusion

The simulation results are very promising and allow to evaluate different geometric constellations of satellites. The amount and placement of satellites have shown to be crucial, especially the selection of a reference satellite having a high elevation is essential for good results. The simulation was also used to determine the sweet spot for the antenna baseline length. Additionally the approach allows to experiment with optimising the solution space and stability of the algorithms. Therefore it is a valuable tool for

further analysis. Applying the developed approach in the described scenarios for automated driving could create a foundation of higher automation while being independent of the Earth's magnetic field.

## IV. OUTLOOK

The constrained dual GNSS approach shown in the previous section is valid when simulated but needs to be verified when used with real measurement data. Using experimental data introduces noise which was neglected in the simulation shown. Consequently no exact solution will be achievable for experimental data which requires optimizing the solution while being aware of potential local minima. Additionally the two independent GNSS receivers need to be synchronized by using the Doppler frequency observations of a corresponding satellite. The synchronisation and general approach of double differencing need to be checked by doing a zero baseline experiment which removes the distance between both antennae by connecting a single antenna to both receivers. The zero baseline experiment should output zero values for all double differences with only small phase residuals and multiples of  $\lambda$ . The simulation results and theory are only valid under the assumption that both receivers sample at exactly the same time, so synchronization is crucial when transitioning towards experimental measurement data.

The scenarios described in the introduction are mostly relevant for automated driving and are especially challenging in urban environments. Therefore combining purely inertial navigation or using a gyroscope for the dual GNSS approach would be beneficial. The combination allows to continuously track heading and also to use each approach to complement the other by checking plausibility and to reject measurement artefacts. For urban environments



it would also help to expand the number of usable satellites by expanding the approach from GPS to other constellations. Having more satellites available creates a basis for even more robust heading estimation since a careful and environment based satellite geometry selection is enabled.



**Lukas Blocher** received his M.Eng. degree in Systems Engineering in 2019. From 2019 to 2020 he was involved in developing localization/AHRS systems for Urban Air Mobility as systems architect. He is currently in the industrial Ph.D. program at Robert Bosch GmbH, Reutlingen, Germany in cooperation with the University of Tuebingen. His focus is on initial heading estimation with inertial and multi-antenna GNSS systems.

## REFERENCES

- [1] Blocher, L., Baklanov, F., Hiller, T., Rocznik M., Gerlach, J. and Bringmann O., *An Experimental Localization Sensor Platform for Enhanced Initial Heading Estimation*, 2020 IEEE Inertial Conference.
- [2] Blocher, L., Mayer, W., Arena, M., Radović, D., Hiller, T., Gerlach, J. and Bringmann O., *Purely Inertial Navigation with a Low-Cost MEMS Sensor Array*, 2021 IEEE Inertial Conference.
- [3] Blocher, L., Mayer, W., Vujadinović, M., Haack, J., Hofele, J., Radović, D., Hiller, T., Gerlach, J. and Bringmann O., *Gyroscope-Aided Odometry Navigation Using a Highly-Precise Automotive MEMS IMU Complemented by a Low-Cost Sensor Array*, 2022 IEEE Inertial Conference.
- [4] Hiller, T., Vujadinović, M., Blocher, L., Mayer, W., Radović, D., *Practical Approaches to Allan Deviation Analysis of Low-Cost MEMS Inertial Sensors*, 2023 IEEE Inertial Conference.
- [5] Hiller, T., Blocher, L., Vujadinovic, M., Pentek, Z., Buhmann, A., Roth, Hubert, *Analysis and Compensation of Cross-Axis Sensitivity in Low-Cost MEMS Inertial Sensors*, 2021 IEEE Inertial Conference.
- [6] Ben-Ari, M., Mondada, F., *Elements of Robotics*, 2017, Springer Nature.
- [7] Bräunl, T. *Embedded Robotics*, 2008, Springer.
- [8] van Brummelen, J., O'Brien, M., Gruyer, D., Najjaran, H., *Autonomous Vehicle Perception: The Technology of Today and Tomorrow*, 2018, Transportation Research Part C: Emerging Technologies.
- [9] van Graas, F., Braasch, M., *GPS Interferometric Attitude and Heading Determination: Initial Flight Test Results*, 1991, Navigation.
- [10] Bonnifait, P.; Bouron, P.; Crubille, P.; Meizel, D., *Data Fusion of Four ABS Sensors and GPS for an Enhanced Localization of Car-like Vehicles*, 2001, Proceedings 2001 ICRA 2001.
- [11] Pentek, Z., Hiller, T., Czmerk, A., *Algorithmic Enhancement of Automotive MEMS Gyroscopes With Consumer-Type Redundancy*, 2021, IEEE Sensors Journal.
- [12] Li, W., Fan, P., Cui, X., Zhao, S., Ma, T., Lu, M., *A Low-Cost INS-Integratable GNSS Ultra-Short Baseline Attitude Determination System*, 2018, MDPI Sensors.
- [13] Lammertsma, P., *Satellite Navigation*, 2005, Institute of Information and Computing Sciences, Utrecht University.
- [14] Van Sickle, J., *GPS for Land Surveyors*, 2015, CRC Press.

